Decentralized Scalable Robust Voltage Control for Islanded AC Microgrids with General Topology

Marjan Shafiee-Rad
Department of Electrical Engineering
Iran University of Science and Technology
Tehran, Iran
shafiee_m@elec.iust.ac.ir

Qobad Shafiee
Department of Electrical Engineering
University of Kurdistan
Kurdistan, Sanandaj, Iran
q.shafiee@uok.ac.ir

Mohammad-Reza Jahed Motlagh
Department of Electrical Engineering
Iran University of Science and Technology
Tehran, Iran
jahedmr@iust.ac.ir

***Abstract*—This paper introduces a scalable decentralized control strategy for the satisfaction of robust stability and robust performance of islanded inverter-interfaced microgrids with the general structure. The proposed control method maintains the stability and the desired performance of the closed-loop system against microgrid topology changes, plug-and-play functionality of DGs, and local load variations. The robust control scheme is formulated in the form of a dynamic output feedback controller for a linear time-invariant system with polytopic-type uncertainty and then converted to an LMI-based convex optimization problem. The capability of the suggested controller is evaluated under several scenarios simulated in MATLAB/SimPowerSystems Toolbox.**

Keywords—inverter-interfaced microgrid, decentralized control, robust stability, robust performance, convex optimization

I. INTRODUCTION

In recent years, distributed generation (DG) units and, subsequently, microgrids have become an essential part of the power networks to make more use of renewable energy sources. As long as the microgrid connects to the main grid, the voltage at the point of common coupling (PCC) and the system frequency are assigned by the main network [1], [2]. Depending on the planned or nonscheduled reasons, the microgrid and the main grid may be disconnected, and the microgrid interns into the islanded (autonomous) mode. In the autonomous mode of operation, microgrid requires a different algorithm to control system frequency and the voltage of the PCC and to prevent instability [3].

The microgrids control schemes in the autonomous operation mode are divided into two general categories, 1) droop-based method [4]-[6], and 2) non-droop-based method [7]-[14]. Droop mechanism is one of the most common control methods for islanded microgrids and is, in fact, a decentralized proportional controller which allows the plug-and-play (PnP) operation of DGs in the microgrid. However, this control methods have some difficulties, such as the compromise between the accuracy of frequency/voltage regulation and power-sharing [6], coupled dynamic between real and reactive power, non-robustness to microgrid topology changes and load variations [4], slow transient response and poor performance in the situation of mixed (resistive-inductive) lines and in the presence of conductance [4], [5].

In recent years, non-droop-based control methods have been proposed to solve the mentioned problems of the droop controllers. In this technique, an internal oscillator controls the frequency of each DG unit, and an advanced dynamic controller regulates the voltage of PCCs [9]. Non-droop-based methods are divided into two general classes, 1) multi-loop state-feedback controllers [11]-[14], and 2) single-loop dynamic output-feedback controllers [7]-[10]. In state-feedback controllers, due to the more need for measuring sensors as well as the availability or estimation of state variables, the overall cost of the system increases, and the system reliability decreases. Therefore, these methods are less appropriate for practical implementation.

One of the main challenges in the islanded microgrid control scheme is the robust stability and robust performance of the closed-loop microgrid against some factors such as microgrid topology changes, PnP functionality of DGs, and also local load variations. The output feedback controllers provided so far have only addressed the robust performance against load changes. These methods have not considered robustness against changes of microgrid topology, and PnP of DG, as well as the modelled microgrid usually does not have an arbitrary structure [7]-[10]. State-feedback controllers have been proposed so far, which in addition to being robust to load changes, have also taken into account robust stability under microgrid topology changes and PnP functionality of DGs [11]-[14]. In the proposed control strategy in [11], [12], whenever a DG is under the PnP functionality, all the local controllers of its neighboring DGs need to be redesigned. Moreover, a three-degree-of-freedom decentralized controller is presented in [13], [14], which does not require to readjust the local controllers due to the PnP functionality of DGs. All of these developed strategies employ state-feedback and two prefilters to improve the output of the closed-loop subsystem and to reduce the load effect. The design of the state-feedback and prefilters are considered as three independent optimization problems. Such an approach will inevitably lead to a suboptimal controller and as a result the suboptimal performance. Also, while the presented controllers assure the robust stability, the robust performance of microgrid is not guaranteed.

This manuscript introduces a new robust output-feedback based controller for the autonomous AC microgrid, including several DGs with general topology. The presented controller maintains the performance and stability of the closed-loop microgrid system against local load variations, system topology changes, and PnP operation of DGs in addition to the satisfying stability and the desired performance of the nominal system. The introduced controller has a decentralized structure providing various advantages such as cost-saving and increased-reliability. The parameters of each local controller are attained from one convex optimization problem, which results in the optimal performance. The successful performance of the recommended controller is verified through several scenarios implemented in MATLAB/SimPowerSystems Toolbox.

978-1-7281-5849-5/20/$31.00 ©2020 IEEE

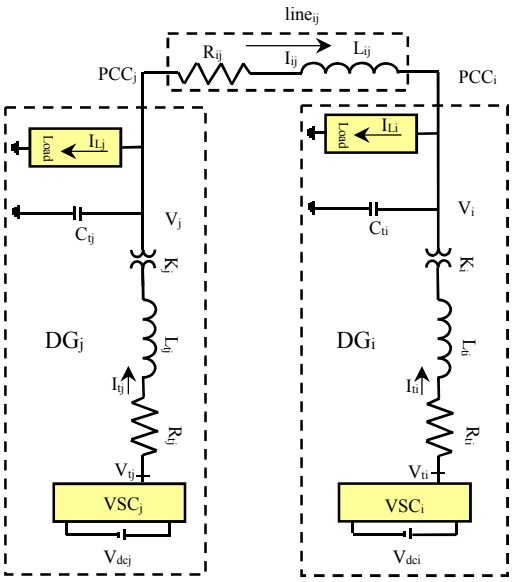

Fig. 1. Electrical circuit of an islanded AC microgrid including two DGs.

This article is categorized as follows: The microgrid model is presented in Section II. The design process of the control system is rendered in Section III. Simulation outcomes are given in Section IV, and the conclusions are propounded in Section V.

II. Mathematical Model of the Islanded Microgrid

In this section, a linear time-invariant (LTI) state-space model for the autonomous AC microgrid has N DGs with general topology is introduced. Each DG includes a voltage-source converter (VSC), an ideal DC voltage source, a step-up transformer with transformation ratio k_i, a series RL filter, a shunt capacitor, and a local load with the measurable current.

First consider a microgrid structure consisting of two DG units, DG i and DG j, connected via a transmission line ij, as shown in Fig. 1. The dynamical equations of the subsystem i (DG i), in the dq-frame, are as follows:

$$DG\ i\begin{cases}\dfrac{dV_{i,dq}}{dt}+j\omega_0 V_{i,dq}=\dfrac{k_i}{C_{ti}}I_{ti,dq}+\dfrac{1}{C_{ti}}I_{ij,dq}-\dfrac{1}{C_{ti}}I_{L_i,dq}\\ \dfrac{dI_{ti,dq}}{dt}+j\omega_0 I_{ti,dq}=-\dfrac{k_i}{L_{ti}}V_{i,dq}+\dfrac{1}{L_{ti}}V_{ti,dq}-\dfrac{R_{ti}}{L_{ti}}I_{ti,dq}\end{cases} \quad (1)$$

$$Line\ ij:\ \frac{dI_{ij,dq}}{dt}+j\omega_0 I_{ij,dq}=-\frac{R_{ij}}{L_{ij}}I_{ij,dq}-\frac{1}{L_{ij}}V_{i,dq}+\frac{1}{L_{ij}}V_{j,dq} \quad (2)$$

where $V_{ti,dq}, I_{ti,dq}, I_{Li,dq}, V_{i,dq}$ and $I_{ij,dq}$ respectively are the dq-components of the VSC terminal voltage, the filter current, the local load current, the PCC voltage, and the transmission line current.

With the Quasi-Stationary Lines (QSL) assumption [15], i.e. $\frac{dI_{ij,dq}}{dt}=0$, the line dynamic and the state-space description of DG i are obtained as follows:

$$I_{ij,dq}=\left(V_{j,dq}-V_{i,dq}\right)/\left(R_{ij}+j\omega_0 L_{ij}\right) \quad (3)$$

$$\begin{cases}\dot{x}_i=A_{ii}x_i+A_{ij}x_j+B_iu_i+B_{w_i}w_i\\ y_i=C_ix_i;\end{cases} \quad (4)$$

where $x_i=[V_{i,d}\quad V_{i,q}\quad I_{ti,d}\quad I_{ti,q}]^T$ is the state vector, $u_i=[V_{ti,d}\quad V_{ti,q}]^T$ is the input, $w_i=[I_{Li,d}\quad I_{Li,q}]^T$ is the exogenous input, and $y_i=[V_{i,d}\quad V_{i,q}]^T$ is the output of DG.

In the same way, if the microgrid system contains N DGs, the state-space equations for DG i are as follows [12]:

$$\begin{cases}\dot{x}_i=A_{ii}x_i+\sum_{j=1,j\neq i}^{N}A_{ij}x_j+B_iu_i+B_{w_i}w_i\\ y_i=C_ix_i;\end{cases}\qquad i=1,\dots,N \quad (5)$$

$$A_{ii}=\begin{bmatrix}-\frac{1}{C_{ti}}\sum_{j=1,j\neq i}^{N}\frac{R_{ij}}{Z_{ij}^2} & \omega_0-\frac{1}{C_{ti}}\sum_{j=1}^{N}\frac{X_{ij}}{Z_{ij}^2} & \frac{k_i}{C_{ti}} & 0\\ -\omega_0+\frac{1}{C_{ti}}\sum_{j=1,j\neq i}^{N}\frac{X_{ij}}{Z_{ij}^2} & -\frac{1}{C_{ti}}\sum_{j=1,j\neq i}^{N}\frac{R_{ij}}{Z_{ij}^2} & 0 & \frac{k_i}{C_{ti}}\\ -\frac{k_i}{L_{ti}} & 0 & -\frac{R_{ti}}{L_{ti}} & \omega_0\\ 0 & \frac{k_i}{L_{ti}} & -\omega_0 & -\frac{R_{ti}}{L_{ti}}\end{bmatrix},$$

$$A_{ij}=\frac{1}{C_{ti}}\begin{bmatrix}\frac{R_{ij}}{Z_{ij}^2} & \frac{X_{ij}}{Z_{ij}^2} & 0 & 0\\ -\frac{X_{ij}}{Z_{ij}^2} & \frac{R_{ij}}{Z_{ij}^2} & 0 & 0\\ 0 & 0 & 0 & 0\\ 0 & 0 & 0 & 0\end{bmatrix},\ B_i=\begin{bmatrix}0 & 0\\ 0 & 0\\ \frac{1}{L_{ti}} & 0\\ 0 & \frac{1}{L_{ti}}\end{bmatrix},$$

$$B_{w_i}=\begin{bmatrix}\frac{-1}{C_{ti}} & 0\\ 0 & \frac{-1}{C_{ti}}\\ 0 & 0\\ 0 & 0\end{bmatrix},\ C_i=\begin{bmatrix}1 & 0 & 0 & 0\\ 0 & 1 & 0 & 0\end{bmatrix} \quad (6)$$

where $\omega_0=2\pi f_0$, $X_{ij}=\omega_0 L_{ij}$, $Z_{ij}^2=R_{ij}^2+\omega_0^2L_{ij}^2$ and f_0 is the nominal frequency of the system, and $A_{ij}=0$ *iff* there exists no junction between DGs i and j.

Finally, the state-space description of the autonomous AC microgrid system is as follows:

$$\begin{bmatrix}\dot{x}_1\\ \dot{x}_2\\ \vdots\\ \dot{x}_N\end{bmatrix}=\begin{bmatrix}A_{11} & A_{12} & \cdots & A_{1N}\\ A_{21} & A_{22} & \cdots & A_{2N}\\ \vdots & \vdots & \ddots & \vdots\\ A_{N1} & A_{N2} & \cdots & A_{NN}\end{bmatrix}\begin{bmatrix}x_1\\ x_2\\ \vdots\\ x_N\end{bmatrix}$$
$$+diag\{B_1,B_2,\dots,B_N\}[u_1\quad\cdots\quad u_N]^T$$
$$+diag\{B_{w_1},B_{w_2},\dots,B_{w_N}\}[w_1\quad\cdots\quad w_N]^T$$
$$[y_1\quad\cdots\quad y_N]^T=diag\{C_1,\dots,C_N\}[x_1\quad\cdots\quad x_N]^T \quad (7)$$

where matrices A_{ii}, A_{ij}, B_i, B_{w_i}, and C_i are as defined in (6).

III. Microgrid Control System Design

The microgrid frequency is controlled by internal oscillators for each DG unit with a fixed frequency at $\omega_0=2\pi f_0$, and through one common-time reference signal the synchronization of all oscillators is achieved.

The expressed state-space model for the whole islanded AC microgrid in (7) represents an interconnected composite system consists of N subsystems, and each one has a state-space description as (5) [16]. Also, it is proved all subsystems (DGs) are controllable and observable, i.e., all controllability matrices $\phi_{Ci}(A_{ii},B_i)$ have full row rank, and all observability

matrices $\phi_{oi}(A_{ii}, C_i)$ have full column rank for all parameters of the system. Therefore, conforming to the outcomes of [16], the interconnected composite system (7) is stabilizable by applying only the local controller for each subsystem (5). Thus, the decentralized control approach is applicable to control the autonomous inverter-interfaced microgrid system with the obtained state-space model (7).

Now for each nominal subsystem, the initial control objectives are, 1) stability, reference voltage tracking, fast transient response, and appropriate control signal, and 2) load disturbance attenuation. The first goal is achieved by the design of a feedback controller $K(s)$, and the second goal is attained via compensating the effect of load current by a feedforward controller $K_w(s)$, as shown in Fig. 2. The transfer functions $G_w(s)$ and $G(s)$ for each DG subsystem are obtained from (5) as follows:

$$\begin{cases} G(s) = C_i(sI - A_{ii})^{-1}B_i \\ G_w(s) = C_i(sI - A_{ii})^{-1}B_{w_i} \end{cases} \tag{8}$$

To reference tracking, an appropriate range of control signal, and disturbance attenuation, the following optimization problems must be solved, respectively to find local controllers $K(s)$ and $K_w(s)$:

$$\begin{aligned} &min\left(\sup\frac{\|e\|_{L_2}}{\|r\|_{L_2}}\right) = min\|T_{re}\|_\infty \\ &= min\|(I + G(s)K(s))^{-1}\|_\infty \end{aligned} \tag{9}$$

$$\begin{aligned} &min\left(\sup\frac{\|u\|_{L_2}}{\|r\|_{L_2}}\right) = min\|T_{ru}\|_\infty \\ &= min\|K(s)(I + G(s)K(s))^{-1}\|_\infty \end{aligned} \tag{10}$$

$$\begin{aligned} &min\left(\sup\frac{\|y\|_{L_2}}{\|w\|_{L_2}}\right) = \min\left\|T_{wy}\right\|_\infty \\ &= min\left\|\left(I + G(s)K(s)\right)^{-1}(G_w + GK_w)\right\|_\infty \end{aligned} \tag{11}$$

Moreover, the weighing filters $W_1(s)$, $W_2(s)$ and $W_w(s)$ can be used in problems (9)-(11) to control the sensitivity function and the bandwidth of the closed-loop system, to restrict the control signal and the effect of the measuring noise, and to properly alleviate the impact of the disturbance input [17], respectively as shown in Fig. 2.

Finally, all control objectives can be expressed as the following optimization problem:

$$\min_{K(s),K_w(s)} \alpha\gamma_1 + \gamma_2$$
$$s.t.\begin{cases} \left\|\dfrac{W_1(s)S(s)}{W_2(s)K(s)S(s)}\right\|_\infty < \gamma_1 \\ \left\|W_w(s)S(s)\left(G_w(s) + G(s)K_w(s)\right)\right\|_\infty < \gamma_2 \end{cases} \tag{12}$$

where α determines a trade-off between the H_∞ performance criterion and the disturbance signal elimination.

By considering the desired controller in the form of $K_c(s) = [K(s) \quad K_w(s)]$, and utilization the state-space model of G_w, G, W_w, W_1 and W_2, the state-space representation of the open-loop system and desired controller are as follows:

$$\begin{bmatrix} \dot{x} \\ z \\ z_m \\ y \end{bmatrix} = \begin{bmatrix} A & B_r & B_w & B \\ C_z & D_{zr} & D_{zw} & D_z \\ C_{z_m} & D_{z_mr} & D_{z_mw} & D_{z_m} \\ C & D_r & D_w & 0 \end{bmatrix} \begin{bmatrix} x \\ r \\ w \\ u \end{bmatrix} \tag{13}$$

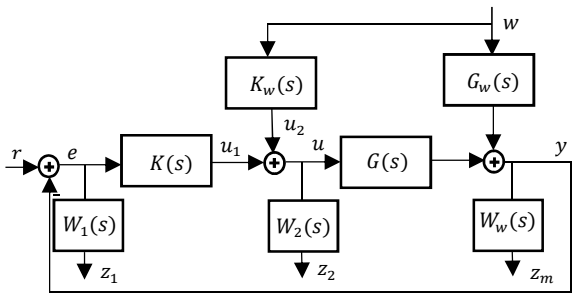

Fig. 2. Block diagram for the presented control manner.

$$\begin{cases} \dot{x}_K = A_K x_K + B_K y \\ u = C_K x_K + D_K y \end{cases} \tag{14}$$

Thus, the state-space description of the close-loop system is obtained as follows:

$$\begin{aligned} \begin{bmatrix} \dot{x} \\ \dot{x}_K \end{bmatrix} &= \begin{bmatrix} A + BD_KC & BC_K \\ B_KC & A_K \end{bmatrix}\begin{bmatrix} x \\ x_K \end{bmatrix} \\ &+ \begin{bmatrix} B_r + BD_KD_r & B_w + BD_KD_w \\ B_KD_r & B_KD_w \end{bmatrix}\begin{bmatrix} r \\ w \end{bmatrix} \\ \begin{bmatrix} z_1 \\ z_2 \\ z_m \end{bmatrix} &= \begin{bmatrix} C_z + D_zD_KC & D_zC_K \\ C_{z_m} + D_{z_m}D_KC & D_{z_m}C_K \end{bmatrix}\begin{bmatrix} x \\ x_K \end{bmatrix} \\ &+ \begin{bmatrix} D_{zr} + D_zD_KD_r & D_{zw} + D_zD_KD_w \\ D_{z_mr} + D_{z_m}D_KD_r & D_{z_mw} + D_{z_m}D_KD_w \end{bmatrix}\begin{bmatrix} r \\ w \end{bmatrix} \end{aligned} \tag{15}$$

Finally, the state-space realization for the constraints of the problem (12) is computable from (15) as follows:

$$\begin{aligned} T_{rz} : &\begin{bmatrix} \hat{A} & \hat{B}_1 \\ \hat{C}_1 & \hat{D}_1 \end{bmatrix} \\ &= \begin{bmatrix} \begin{pmatrix} A + BD_KC & BC_K \\ B_KC & A_K \end{pmatrix} & \begin{pmatrix} B_r + BD_KD_r \\ B_KD_r \end{pmatrix} \\ (C_z + D_zD_KC \quad D_zC_K) & D_{zr} + D_zD_KD_r \end{bmatrix} \end{aligned} \tag{16}$$

$$\begin{aligned} T_{wz_m} : &\begin{bmatrix} \hat{A} & \hat{B}_2 \\ \hat{C}_2 & \hat{D}_2 \end{bmatrix} \\ &= \begin{bmatrix} \begin{pmatrix} A + BD_KC & BC_K \\ B_KC & A_K \end{pmatrix} & \begin{pmatrix} B_w + BD_KD_w \\ B_KD_w \end{pmatrix} \\ (C_{z_m} + D_{z_m}D_KC \quad D_{z_m}C_K) & D_{z_mw} + D_{z_m}D_KD_w \end{bmatrix} \end{aligned} \tag{17}$$

From (17) and (18), the constraints description is equivalent to a state-space representation of an LTI system with a dynamic output-feedback controller.

For PnP modeling, a similar approach to the method outlined in [13] with some improvement is used. The goal is to make the stability and performance of all DGs robust after each PnP occurrence. In other words, with the entry or exit of DG i, the same unit i and other DGs must have satisfactory performance. According to the state-space matrices defined in (6), it is clear that with PnP of DG i, only the matrix A_{ii} for DG i and other DGs that are connected to it, change. In fact, matrix A_{ii} has polytopic-type uncertainty structure with two uncertain parameters as follows:

$$A_{ii} = \begin{bmatrix} q_1 & q_2 & \dfrac{k_i}{C_{ti}} & 0 \\ -q_2 & q_1 & 0 & \dfrac{k_i}{C_{ti}} \\ \dfrac{-k_i}{L_{ti}} & 0 & \dfrac{-R_{ti}}{L_{ti}} & \omega_0 \\ 0 & \dfrac{k_i}{L_{ti}} & -\omega_0 & \dfrac{-R_{ti}}{L_{ti}} \end{bmatrix} \tag{18}$$

Moreover, two cases for each uncertain element is considered as follows:

$$q_j^{min} \le q_j \le q_j^{max} \quad j = 1,2 \tag{19}$$

where the minimum/maximum value of q_j calculated as:

- q_j^{max}: Maximum possible connection of DGs to DG i.
- q_j^{min}: Disconnection of all lines connected to DG i and according to (6) $q_1^{min} = 0,\ q_2^{min} = -\omega_0$.

Therefore, the convex hull of uncertain matrix A_{ii} has four vertices, and each conceivable connection or disconnection of other DGs to DG i falls into a polytopic region, as follows:

$$\begin{aligned} A_{ii}^1 &= A_{ii}(q_1^{min}, q_2^{min}), A_{ii}^2 = A_{ii}(q_1^{min}, q_2^{max}) \\ A_{ii}^3 &= A_{ii}(q_1^{max}, q_2^{min}), A_{ii}^4 = A_{ii}(q_1^{max}, q_2^{max}) \end{aligned} \tag{20}$$

$$A_{ii}(q_1, q_2) = \sum_{j=1}^{2^2} \theta_j A_{ii}^j, \quad \sum_{j=1}^{2^2} \theta_j = 1, \quad \theta_j \ge 0 \tag{21}$$

Thus, the PnP functionality is modeled as a polytopic-type uncertainty with four vertices in the matrix A_{ii} and consequently in the closed-loop matrix $\hat{A}_i$.

Since all possible scenarios of connecting DG units together are considered in the convex hull that proposed for PnP modelling, if some transmission lines are disconnected, the polytopic uncertainty region and its vertices will not change. Consequently, this approach is also robust to microgrid topology changes.

According to the explanations and relations presented in this section, the final issue is the design of the dynamic output-feedback controller with H_∞ performance criteria for an LTI system with a polytopic uncertainty in matrix A. The design should be done by solving a convex optimization problem by satisfying a set of LMI constraints in the polytopic vertices. To reduce the conservatism related to a common Lyapunov matrix for the whole uncertain space, using a linearly parameter-dependent (LPD) Lyapunov matrix is a suitable choice. Various algorithms are proposed to solve this nonconvex optimization problem using LPD Lyapunov function based on the development of Bounded Real Lemma (BRL), and the method outlined in [10] is used here.

The robust performance and the robust stability of the closed-loop DG subsystem given in (16) and (17) under the fixed-order local controller of (14) are satisfied, through the following convex optimization problem [10]:

$$min_{P_1^j, P_2^j, A_K, B_K, C_K, D_K} \quad \alpha\gamma_1 + \gamma_2$$

$$s.t.: \begin{cases} \begin{bmatrix} M^T P_1^j & * & * & * \\ P_1^j - M + T^{-1}\hat{A}^j T & -2I & * & * \\ 0 & (T^{-1}\hat{B}_1)^T & -I & * \\ \hat{C}_1 & 0 & \hat{D}_1 & -\gamma_1 I \end{bmatrix} < 0 \\ \begin{bmatrix} M^T P_2^j & * & * & * \\ P_2^j - M + T^{-1}\hat{A}^j T & -2I & * & * \\ 0 & (T^{-1}\hat{B}_2)^T & -I & * \\ \hat{C}_2 & 0 & \hat{D}_2 & -\gamma_2 I \end{bmatrix} < 0 \\ P_1^j, P_2^j > 0 \qquad j = 1, \dots, 4 \end{cases} \tag{22}$$

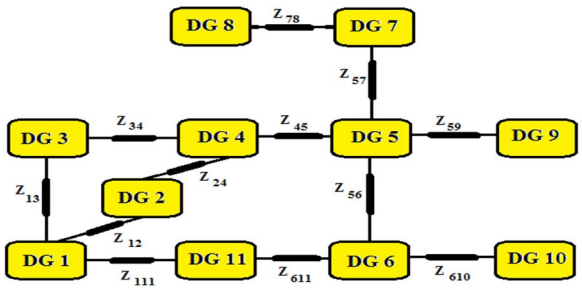

Fig. 3. Configuration of the test autonomous microgrid.

where T and M are two slack matrices obtained from:

$$\begin{aligned} T &= (chol(X))^{-1} \\ M &= T^T M_T T \end{aligned} \tag{23}$$

where $chol$ indicates Cholesky factorization and (M_T, X) obtained from the following convex problem:

$$min_{P_T^j, X, M_T} \quad \gamma$$

$$s.t. \begin{cases} \begin{bmatrix} \tilde{A}^{jT} P_T^j + P_T^j \tilde{A}^j & * & * & * \\ P_T^j + M_T - X\tilde{A}^j & -2X & * & * \\ -\tilde{B}^T M_T + \tilde{B}^T X \tilde{A}^j & \tilde{B}^T X & -I & * \\ \tilde{C}^T & 0 & \tilde{D}^T & -\gamma I \end{bmatrix} < 0 \\ P_T^j > 0 \qquad j = 1, \dots, 4 \end{cases} \tag{24}$$

where $(\tilde{A}^j, \tilde{B}, \tilde{C}, \tilde{D})$ are the state-space matrices of the jth vertex of the closed-loop system obtained from (15).

It should be noted that an iterative procedure is needed to solve the convex optimization problem (22) for each DG subsystem and attain the state-space realization of the corresponding local output-feedback controller $K_c(s)$. In other words, after designing the initial controller, the slack matrices are extracted from (24) and (23), then the convex optimization problem (22) is solved to update the controller parameters. This process continues until convergence or reaching the maximum iterations number. It has been shown that the reduced-order controller (22) attends to a monotonous convergence of the H_∞ norm upper-bound [10].

IV. Simulation Results

In this part, the capability of the recommended controller to maintain the stability and the desired performance of the closed-loop microgrid system is evaluated through several scenarios. The presented controller has been applied to a microgrid with 11 DGs [12], as shown in Fig. 3. The electrical parameters of the microgrid are given in [13]. The microgrid is simulated in MATLAB/SimPowerSystems Toolbox, and local controllers are calculated from solving the convex optimization problem (22) via YALMIP [18].

A. Nominal Performance of the Closed-Loop System

This subsection evaluates the stability and the desired performance of the nominal microgrid system. To this end, at $t = 1.5s$, the d and q reference voltage components for DG 6 respectively altered from 0.6 pu and 0.8 pu to o.8 pu and 0.6 pu. Fig. 4 displays the dynamic response of DG 6 due to the reference voltages change. As it can be seen in Fig. 4, the output voltages track the reference values quickly with zero steady-state error, low interaction between the channels and repulsion of high-frequency harmonics caused by switching. The control signal amplitude is also suitable.

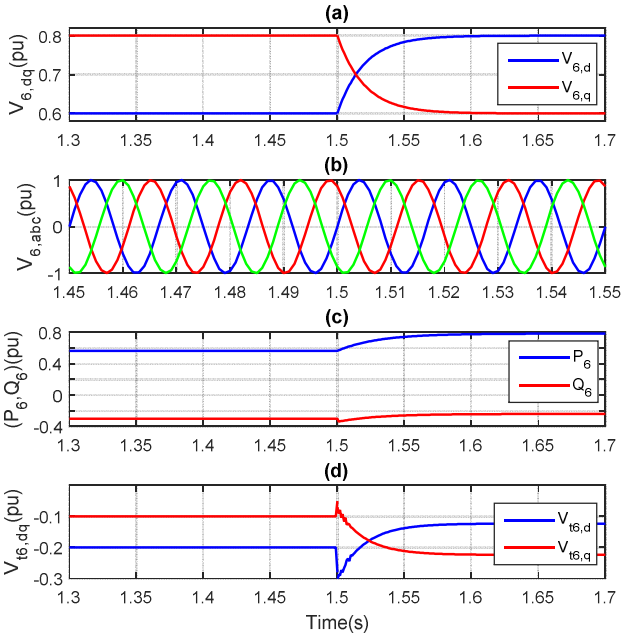

Fig. 4. Dynamic response of nominal system due to the change in reference voltage of DG 6 (a) dq components of PCC voltage, (b) abc components of PCC instantaneous voltage, (c) output powers, and (d) dq components of control signal.

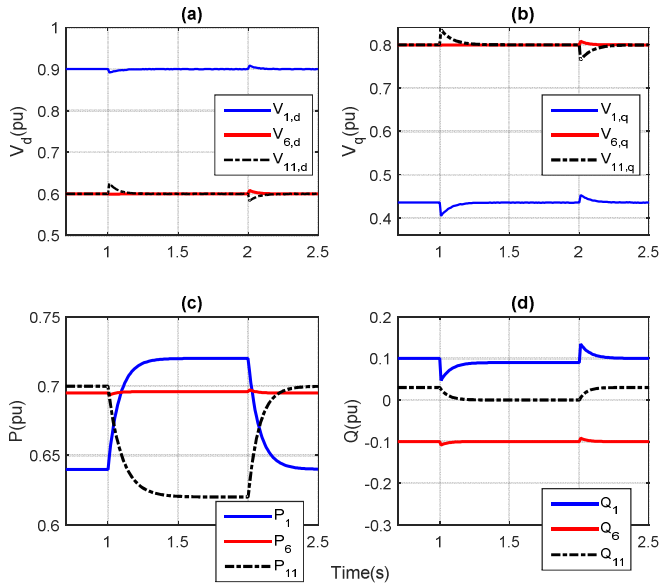

Fig. 5. Dynamic responses of DG 11 and its neighbours under the PnP operation of DG 11 (a) d-component of voltage signals, (b) q-component of voltage signals, (c) output real powers, and (d) output reactive powers.

The rise-time of the output voltage at PCC with the proposed controller is about three cycles of f_0 that is acceptable based on the IEEE standard [19]. The obtained results show that the system response is better than previously provided robust state-feedback controllers due to the optimized design of the suggested decentralized controller [12], [13].

B. Robustness to PnP Functionality of DGs

This scenario examines the robust performance of the microgrid closed-loop system against the PnP operation of DGs. Presume that DG 11 is plugged out from the microgrid at $t = 1s$ and then plugged into the system at $t = 2s$. Hence, the dynamics of DGs 6 and 1 vary too.

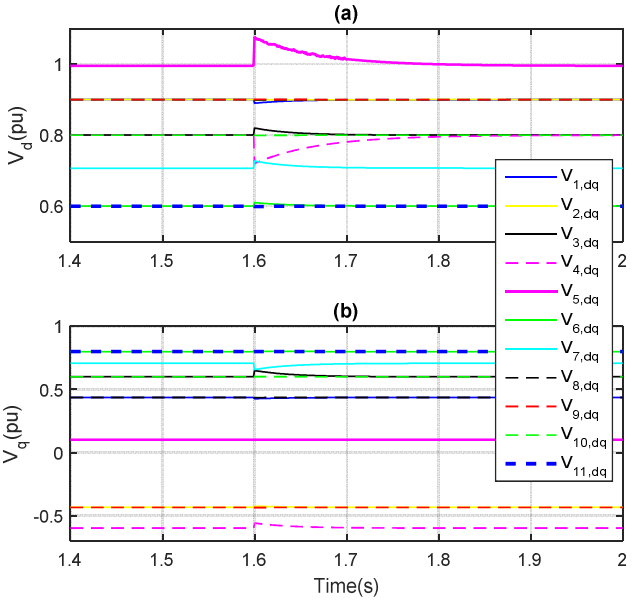

Fig. 6. Dynamic responses of all DGs due to the microgrid topology changes at $t = 1.6s$ (a) d-component of voltage signals, and (b) q-component of voltage signals.

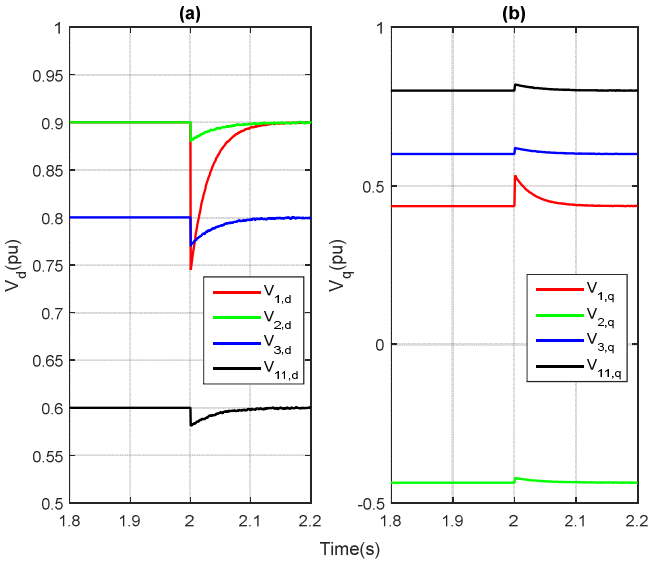

Fig. 7. Dynamic responses of DG 1 and its neighbours due to the PCC 1 load change at $t = 2s$ (a) d-component of voltage signals, and (b) q-component of voltage signals.

Fig. 5 shows the dynamic responses of DG 11 and its neighbours due to these PnP functionalities. The results demonstrate the local controllers regulate the load voltages after the PnP operation with a fast transient response and zero steady-state error. The transient response is also faster than previous robust methods [13]. In other words, the recommended control method keeps the stability and the desired performance of the closed-loop system based on the IEEE standard [19] under the PnP operation of DGs, i.e., it does not need to redesign of the local output-feedback controllers.

C. Robustness to Microgrid Topology Changes

In this subsection, the performance of the closed-loop system under the designed controller is evaluated against changes in microgrid topology. To this end, the lines between DGs 4 and 5, and DGs 3 and 1 are disconnected at $t = 1.6s$.

Fig. 6 indicates the output voltages of all DGs to these variations and demonstrates that after this change the local controllers were able to adjust the output load voltages with zero steady-state error quickly compared to the robust methods already presented [13]. Thus, the proposed control strategy is strongly robust to uncertainties affecting the microgrid topology.

D. Robustness to Local Load Variations

This part assays the performance of the designed controller against local load changes. The loads at PCCs are in the form of a parallel RLC network. The load resistance at PCC 1 is modified from 152Ω to 76Ω at $t = 2s$ in the three-phase. The output voltages of DG 1 and its neighbours due to this change are shown in Fig. 7. The results show that the stability and performance of the microgrid are maintained against load changes with a fast and limited transient.

V. Conclusion

In this work, a new robust scalable controller for the islanded inverter-interfaced microgrid, including several DGs with general topology, is presented. The proposed controller has a decentralized structure and uses output-feedback, which reduces costs and increases the reliability of the system. Some capabilities of the controller are the closed loop system stability, zero steady-state error, appropriate transient response, a proper control signal, bandwidth regulation of the closed loop system, restricting of measurement noise, and disturbance compensation. The suggested control scheme provides the stability and the desired performance of the closed loop system under nominal conditions and also against some changes such as PnP of DGs, microgrid topology changes, and loads variations. Unlike the previously presented robust state-feedback controllers, each provided local controller is a solution of one convex LMI-based problem, which results in the optimal performance. The success of the suggested robust controller in maintaining the stability and the desired performance of the microgrid is verified through several scenarios.

References

[1] D. E. Olivares, A. Mehrizi-Sani, A. H. Etemadi, C. A. Canizares, R. Iravani, M. Kazerani, A. H. Hajimiragha, O. Gomis-Bellmunt,M. Saeedifard, R. Palma-Behnke, G. A. Jimenez-Estevez, and N. D. Hatziargyriou, "Trends in microgrid control," *IEEE Trans. Smart Grid*, vol. 5, no. 4, pp. 1905-1919, Jul. 2014.

[2] J. M. Guerrero, M. Chandorkar, T. Lee, and P. C. Loh, "Advanced control architecture for intelligent microgrids-Part I: Decentralized and hierarchical control," *IEEE Trans. Ind. Electron.*, vol. 60, no. 4, pp. 1254-1262, Apr. 2013.

[3] "IEEE Standard for Interconnecting Distributed Resources with Electric Power Systems," in *IEEE Std 1547-2003*, ed, 2003.

[4] M. Savaghebi, A. Jalilian, J. C. Vasquez, and J. M. Guerrero, " Autonomous voltage unbalance compensation in an islanded droop-controlled microgrid," *IEEE Trans. Ind. Electron.*, vol. 60, no. 4, pp. 1390-1402, Nov. 2013.

[5] J. Schiffer, R. Ortega, A. Astolfi, J. Raisch, and T. Sezi, "Conditions for stability of droopcontrolled inverter-based microgrids, " *Automatica,* vol. 50, no. 10, pp. 2457-2469, Oct. 2014.

[6] Q. C. Zhong, "Robust droop controller for accurate proportional load sharing among inverters operated in parallel," *IEEE Trans. Ind. Electron.*, vol. 60, no. 4, pp. 1281-1290, Apr. 2013.

[7] M. Hamzeh, S. Emamian, H. Karimi, and J. Mahseredjian, "A robust control of an islanded microgrid under unbalanced and nonlinear load conditions," *IEEE J. Emerg. Sel. Topics Power Electron.*, vol. 4, no. 2, pp. 512-520, Jun. 2016.

[8] M. Babazadeh, and A. Nobakhti, " Robust decomposition and structured control of an islanded multi-DG microgrid," *IEEE Trans. Smart Grid,* vol. 10, no. 3, pp. 2463-2474, May 2019.

[9] H. R. Baghaee, M. Mirsalim, G. Gharehpetian, and H. A. Talebi "A decentralized robust mixed $H_2 - H_\infty$ voltage control scheme to improve small/large-signal stability and FRT capility of islanded multi-DER microgrids considering load disturbances," *IEEE Syst. J.,* vol. 12, no. 3, pp. 2610-2621, Sep. 2018.

[10] M. S. Sadabadi, A. Karimi, H. Karimi, "Fixed-order decentralized /distributed control of islanded inverter-interfaced microgrids, " *Control Engineering Practice*, vol. 45, pp. 174-193, Dec. 2015.

[11] S. Riverso, F. Sarzo, and G. Ferrari-Trecate, "Voltage and frequency control of islanded microgrids: A plug-and-play approach," in *IEEE Int. Conf. Smart Grid Com.*, Venice, Italy, pp. 73-78, Nov. 2014.

[12] S. Riverso, F. Sarzo, and G. Ferrari-Trecate, "Plug-and-play voltage and frequency control of islanded microgrids with meshed topology," *IEEE Trans. Smart Grid*, vol. 6, no. 3, pp. 1176-1184, May 2015.

[13] M. S. Sadabadi, Q. Shafiee, A. Karimi, " Plug-and-Play voltage stabilization in inverter-interfaced microgrids via a robust control strategy," *IEEE Trans. Control Syst. Technol.*, vol. 25, no. 3, pp. 781-791, May 2017.

[14] M. S. Sadabadi, Q. Shafiee, A. Karimi, "Plug-and-play robust voltage control of DC microgrids," *IEEE Trans. Smart Grid*, vol. 9, no. 6, pp. 6886-6896, Nov. 2018.

[15] V. Venkatasubramanian, H. Schattler, and J. Zaborszky, "Fast time-varying phasor analysis in the balanced three-phase large electric power system," *IEEE Trans. Automat. Control,* vol. 40, no. 11, pp. 1975-1982, Nov. 1995.

[16] E. J. Davison, "The robust decentralized control of a general servomechanism problem," *IEEE Trans. on Automatic Control*, vol. 21, no. 1, pp. 14-24, Feb. 1976.

[17] S. Skogestad and I. Postlethwaite, Multivariable Feedback Control: Analysis and Design. Hoboken, NJ: Wiley, 2001.

[18] J. L¨ofberg, "YALMIP: A toolbox for modeling and optimization in MATLAB," in *Proc. IEEE Int. Symp. Comp. Cont. Syst. Design (CACSD)*, 2004. [Online]. Available: http://control.ee.ethz.ch/ ~joloef/yalmip.php

[19] "IEEE recommended practice for monitoring electric power quality, IEEE standard 1159," 2019.